HHS Public Access

Author manuscript

Sci Transl Med. Author manuscript; available in PMC 2023 February 14.

Published in final edited form as:

Sci Transl Med. 2022 October 05; 14(665): eabo1050. doi:10.1126/scitranslmed.abo1050.

A germline SNP in BRMS1 predisposes patients with lung adenocarcinoma to metastasis and can be ameliorated by targeting c-fos

Yuan Liu[1,2], **Neel Chudgar**[1], **Brooke Mastrogiacomo**[1,3], **Di He**[1], **Manendra B. Lankadasari**[1], **Samhita Bapat**[1], **Gregory D. Jones**[1], **Francisco Sanchez-Vega**[3], **Kay See Tan**[4], **Nikolaus Schultz**[3], **Semanti Mukherjee**[5], **Kenneth Offit**[5], **Yongde Bao**[6], **Matthew J. Bott**[1,3], **Natasha Rekhtman**[2,7], **Prasad S. Adusumilli**[1,2], **Bob T. Li**[2,5], **Marty W. Mayo**[8], **David R. Jones**[1,2,*]

[1]Thoracic Service, Department of Surgery, Memorial Sloan Kettering Cancer Center; New York, NY 10065, USA

[2]Druckenmiller Center for Lung Cancer Research, Memorial Sloan Kettering Cancer Center; New York, NY 10065, USA

[3]Center for Molecular Oncology, Memorial Sloan Kettering Cancer Center; New York, NY USA

[4]Department of Epidemiology and Biostatistics, Memorial Sloan Kettering Cancer Center; New York, NY 10065, USA

[5]Department of Medicine, Memorial Sloan Kettering Cancer Center; New York, NY 10065, USA

[6]Department of Microbiology, University of Virginia; Charlottesville, VA 22908, USA

[7]Department of Pathology, Memorial Sloan Kettering Cancer Center; New York, NY 10065, USA

[8]Department of Biochemistry & Molecular Genetics, University of Virginia; Charlottesville, VA 22908, USA

Abstract

[*]**Corresponding Author:** David R. Jones, MD, Professor & Chief, Thoracic Service, Department of Surgery, Memorial Sloan Kettering Cancer Center, 1275 York Avenue, Box 7, New York, NY 10065 USA Phone: 212-639-6428; Fax: 232-639-6686; jonesd2@mskcc.org.

Author contributions:

Y.L. conceived the project, obtained the funding, designed the experiments, performed in vitro and in vivo experiments, analyzed and interpreted the data, and wrote and revised the paper. N.C. constructed the plasmids encoding BRMS1 v2 and established A549 and H1299 stable cell lines, performed invasion and tail-vein injection metastasis assays using A549 and H1299 stable cell line. B.M., F.S.V and N.S. participated in bioinformatics analyses and reviewed and edited the paper. K.S.T. was responsible for statistical analyses and reviewed and edited the paper. S.B. performed Taqman SNP assays and Sanger sequencing for *BRMS1v2* in LUAD specimens, carry out the Western blot and quantitative RT-PCR, participated in PDOs maintenance, and supported the animal experiments. G.D.J., D.H. and M.B.L reviewed and edited the paper. Y.B. performed next-generation sequencing for *BRMS1*. N.R. supported in histologic analyses for human LUAD specimens and PDOs. S.M. helped obtain the data of SNP rs1052566 incidence. M.J.B. and B.T.L supported in data interpretation and reviewed and edited the paper. K.O. supported in conceiving the project and designing the experiments. P.S.A. obtained the funding and reviewed and edited the paper. M.W.M obtained the funding, conceived the project, designed the experiment, interpreted the data, and reviewed and edited the paper. D. R. J. obtained the funding, conceived the project, designed the experiment, interpreted the data, and wrote and revised the paper.

Data and materials availability:

All data are available in the main text or the supplementary materials from Dr. David Jones' laboratory under a material transfer agreement with Memorial Sloan Kettering Cancer Center. RNA-seq data have been deposited in the Gene Expression Omnibus database under the accession number GSE. The code for RNA-seq analysis including the upstream packages from the core analysis:STAR aligner (2-pass method) DOI: 10.1093/bioinformatics/bts635; Count matrices: HT-seq counts DOI: 10.1093/bioinformatics/btu638; and the packages used for downstream RNA seq analysis: DESeq2 DOI: 10.1186/s13059-014-0550-8.

Approximately 50% of patients with early-stage, surgically resected lung cancer will develop distant metastasis. There remains an unmet need to identify patients likely to develop recurrence and to design innovative therapies to decrease this risk. Two primary isoforms of BRMS1, v1 and v2 are present in humans. Using next generation sequencing of *BRMS1* on matched human noncancerous lung tissue and NSCLC specimens we identified single-nucleotide polymorphism rs1052566 that results in an A273V mutation of BRMS1v2. This SNP is homozygous (*BRMS1v2*$^{A273V/A273V}$) in 8% of the population and correlates with aggressive biology in lung adenocarcinoma (LUAD). Mechanistically we show that BRMS1v2 A273V abolishes the metastasis suppressor function of BRMS1v2 and promotes robust cell invasion and metastases by activation of c-fos-mediated gene-specific transcriptional regulation. BRMS1v2 A273V increases cell invasion in vitro and increases metastases in both tail-vein injection xenografts and LUAD patient-derived organoid (PDO) intracardiac injection metastasis in vivo models. Moreover, we show that BRMS1v2 A273V fails to interact with nuclear Src, thereby activating intratumoral c-fos in vitro. Higher c-fos results in upregulation of *CEACAM6*, which drives metastases in vitro and in vivo. Using both xenograft and PDO metastasis models, we repurposed T5224, a c-fos pharmacologic inhibitor investigated in clinical trials for arthritis, and observed suppression of metastases in *BRMS1v2*$^{A273V/A273V}$ LUAD in mice. Collectively, we elucidate the mechanism of *BRMS1v2*$^{A273V/A273V}$-induced metastases and offer a putative therapeutic strategy for patients with LUAD who have this germline alteration.

One Sentence Summary:

A homozygous germline alteration, *BRMS1v2*$^{A273V/A273V}$, results in increased c-fos-mediated metastases in lung adenocarcinoma.

INTRODUCTION

In 2020, lung cancer was diagnosed in 2.1 million people worldwide and accounted for 1.8 million deaths—the highest mortality of all solid tumor malignancies(1). Approximately 50% of patients with lung cancer present with metastatic disease(2). However, even among patients with earlier-stage disease who undergo complete surgical resection and adjuvant chemotherapy, up to 50% will inevitably develop metastatic disease(3). Given the clinical heterogeneity of outcomes after definitive therapy, there remains an unmet need to identify patient and tumor risk factors that predispose to the development of metastases.

The use of next-generation sequencing in clinical practice has led to the identification of specific “driver” tumor genomic perturbations in *EGFR, ALK, HER2, ROS1, MET, BRAF, NTRK*, and other genes linked to tumor initiation, growth, and progression in non-small cell lung cancer (NSCLC)(4–6). A secondary, and underexplored, aspect of next-generation sequencing tumor profiling is the ability to examine germline DNA alterations and their associations with disease. Candidate gene studies as well as genome-wide association studies have identified germline mutations that are associated with susceptibility to lung cancer or inherited lung cancer syndromes(7, 8). A handful of single-nucleotide polymorphisms (SNPs)—including those in the *MMP9* coding region(9), the *SIPA1* promoter(10), and the *PI3K-PTEN-mTOR*(11) and *TGFβ*(12, 13) signaling pathways—have been reported to be associated with aggressive lung cancer phenotypes. Heretofore, nearly

all investigations of genetic vulnerabilities have focused on susceptibility and sensitivity to therapy; the contributions of SNPs to the biology of metastases in NSCLC have not been examined.

We and others have shown that BRMS1 suppresses metastases in NSCLC and other solid tumor malignancies(14–16) through its ability to function in a multiprotein histone deacetylase transcriptional corepressor complex(17, 18) or as an E3 ligase to control protein degradation of p300 acetyltransferase (19). Two major transcripts are encoded by the *BRMS1* locus, *BRMS1* isoform 1 (*BRMS1v1*, 246 aa) and *BRMS1* isoform 2 (*BRMS1v2*, 290 aa), which encodes an additional 44 aa at the C-terminus owing to its alternative splicing. Previous studies have focused on related mechanisms through which BRMS1v1 suppresses metastases(17–19). However, the BRMS1v2 isoform has not been thoroughly studied, and its role in cancer progression is unknown.

In this study, we show that homozygous SNP rs1052566 results in a missense mutation at codon 273 (Ala to Val) in BRMS1v2 (*BRMS1v2*$^{A273V/A273V}$) and is present in 8% of individuals of European ancestry and 28% of South Asians. *BRMS1v2*$^{A273V/A273V}$ is associated with a higher risk of metastases and worse progression-free survival (PFS) in patients with early-stage disease. The evidence provided here using CRISPR knock-in isogenic lung adenocarcinoma (LUAD) cells and patient-derived organoids (PDOs) indicates that *BRMS1v2*$^{A273V/A273V}$ promotes invasion and the development of tumor metastases through c-fos–dependent prometastatic processes. Our data suggest that individuals harboring homozygotic *BRMS1v2*$^{A273V/A273V}$ have a predisposition for developing metastatic LUAD and that *BRMS1v2*$^{A273V/A273V}$ could potentially serve as a biomarker to predict the development of metastatic disease in patients with early-stage LUAD. Finally, using a PDO metastasis model, we show that pharmacologic targeting of c-fos in *BRMS1v2*$^{A273V/A273V}$ LUAD results in fewer metastases in vivo. This highlights *BRMS1v2*$^{A273V/A273V}$ as a potential target for therapeutic strategies in patients with LUAD with this germline alteration.

RESULTS

Homozygous SNP *rs1052566* identifies patients at risk for LUAD metastases.

Although somatic mutations in the *BRMS1* locus are rare (cBioportal.org), 2955 SNPs have been identified (dbSNP; www.ncbi.nlm.nih.gov/SNP/). To date, no clinical significance has been reported for these SNPs. Using matched human noncancerous lung tissue and NSCLC specimens, we identified 25 SNPs in exons of *BRMS1*; of these, rs1052566 (G>A) in exon 10 is the only polymorphism that causes the A273V missense mutation in BRMS1v2 (Fig. S1A and fig. 1A). The frequency of the A allele (GA and AA) in The Cancer Genome Atlas (TCGA) LUAD cohort was 27%, with homozygous AA (*BRMS1v2*$^{A273V/A273V}$) present in 8.2% of patients (Fig. 1B). We confirmed similar incidences of rs1052566 in our own LUAD cohort (Fig. S1B). Similarly, the frequency of the A allele (GA and AA) was 26% and the frequency of AA was 7.1% in the TCGA breast cancer cohort (Fig. S1C). Collectively, the incidence of the A allele of rs1052566 in the TCGA cohorts was similar to that reported in dbSNP (22%-30%).

We next investigated whether rs1052566 was associated with tumor recurrence by examining the PFS of patients with LUAD without metastatic disease (surgically resected, stage I-II, nodenegative disease; Fig. 1C and fig. S1D) in the TCGA cohort. We selected this cohort of patients to exclude the impact of oncogenic alterations and loss of heterozygosity during disease progression(3, 20). In addition, 80% of the TCGA cohort had pathologic stage I-II disease. Patients harboring tumors with AA (*BRMS1v2*$^{A273V/A273V}$) were more likely to develop metastatic disease and had worse PFS, compared with patients with tumors with GG and GA (Fig. 1C and fig. S1D). In addition, no difference in the incidence of *BRMS1v2*$^{A273V/A273V}$ in patients with different pathologic stages of LUAD was observed. However, among patients with breast cancer, *BRMS1v2*$^{A273V/A273V}$ was more frequently observed in those with advanced-stage or nodal disease, compared with early-stage or node-negative disease, respectively (Fig. S1E).

BRMS1v2$^{A273V/A273V}$ promotes aggressiveness in LUAD.

BRMS1v2, like BRMS1v1, is expressed in human LUAD (Figs. 1D and 1E). To explore the function of BRMS1v2 and the impact of BRMS1v2 A273V in LUAD, LUAD cells stably expressing ectopic V5-epitope BRMS1v2 wild-type (WT) or A273V mutant were generated (Fig. S2A). In contrast to BRMS1v1, which is present in the nuclei and cytoplasm, BRMS1v2 is primarily nuclear (Fig. 1E, and figs. S2, B and C), which suggested BRMS1v2 may function differently from BRMS1v1. Ectopic BRMS1v2 WT or A273V mutant did not affect cell growth (Fig. S2D). However, cells with V5-BRMS1v2 A273V exhibited an elongated, mesenchymal morphologic appearance with increased stress fiber formation, whereas cells with V5-BRMS1v2 WT had a more cobblestone, epithelioid shape (Fig. S2E). Ectopic BRMS1v2 A273V promoted invasion of LUAD cells (Fig. 1F). To further investigate whether BRMS1v2 affects LUAD metastasis in vivo, we used a tail-vein injection metastasis model of WT and mutant BRMS1v2 A549 cells into nude mice. No cancer colonization was observed in the BRMS1v2 WT group (n=0/10); however, the incidence of metastatic colonization was higher in the BRMS1v2 A273V group (n=6/10) (Fig. 1G). Collectively, our data suggest that BRMS1v2 WT suppresses lung cancer metastases, whereas BRMS1v2 A273V increases cell invasion in vitro and lung cancer metastases in vivo.

To elucidate the functional mechanisms of *BRMS1v2*$^{A273V/A273V}$ in LUAD, we used a CRISPR knock-in approach to generate two clones of LUAD H358 *BRMS1v2*$^{WT/A273V}$ (named H1 and H2, Fig. S3A) and *BRMS1v2*$^{A273V/A273V}$ isogenic cells (named clones C1 and C2; Fig. 2A). H358 cells were chosen because there is no identified genomic alteration in the *BRMS1* locus. Consistent with observations in LUAD cells (Fig. S2E), both C1 and C2 cells exhibited an elongated, mesenchymal morphologic appearance, compared with parental cells (*BRMS1v2*$^{WT/WT}$) and *BRMS1v2*$^{WT/A273V}$ isogenic cells (Fig. 2B and fig. S3A). Although no difference in cell growth was observed between *BRMS1v2*$^{A273V/A273V}$ isogenic and parental cells (Fig. S3B), *BRMS1v2*$^{A273V/A273V}$ cells had higher cell migration (Fig. 2C), invasion after 2-D (Fig. 2D and fig. S3C) and 3-D (Fig. 2E) culturing, and formation of cell spheroids (Fig. 2F and fig. S3D), compared with parental cells and *BRMS1v2*$^{WT/A273V}$ isogenic cells. Collectively, our data reveal that, similar to BRMS1v1, BRMS1v2 WT suppresses metastases. However, BRMS1v2 A273V

appears to promote aggressiveness of LUAD cells, including higher amounts of migration, invasion, and stemlike cell growth.

c-fos is increased in *BRMS1v2*$^{A273V/A173V}$ isogenic cells.

To investigate the mechanisms through which *BRMS1v2*$^{A273V/A273V}$ affects LUAD cell metastases, we performed RNA-seq using H358 parental and related *BRMS1v2*$^{A273V/A273V}$ isogenic clones. We identified 164 and 123 genes differentially expressed, compared with parental cells, in C1 and C2 cells, respectively (log_2 fold change [FC] >1 and $P<0.05$; Fig. 3, A and B, and fig. S4A). Whereas *BRMS1v2*$^{A273V/A273V}$ isogenic cells exhibited mesenchymal morphologic appearance (Fig. 2B), the mRNAs of epithelial-mesenchymal transition (EMT) hallmark genes(21) were not upregulated in C1 and C2 cells, compared to parental cells (Fig. S4B). To identify upstream pathways associated with the overlapping upregulated genes between C1 and C2 clones, transcription factor binding signature (UCSC_TFBS) analysis in The **D**atabase for **A**nnotation, **V**isualization and **I**ntegrated **D**iscovery (**DAVID** 2021, https://david.ncifcrf.gov/) (22) was performed. AP-1 was the top transcription factor by which the most genes (73.5%) were putatively up-regulated (Fig. 3B). Given that c-fos and c-Jun are the most common members of the AP-1 transcription factor family (23), we assessed mRNA expression in *BRMS1v2*$^{A273V/A273V}$ isogenic cells and found no difference compared with *BRMS1v2*$^{WT/WT}$ cells (Fig. S4C). Total and active (p-c-fos S32) c-fos protein, but not c-Jun, were higher in isogenic cells, compared with WT cells (Fig. 3C). c-fos was also higher in cells with V5-BRMS1v2 A273V than in cells with V5-BRMS1v2 WT (Fig. S4D). Collectively, these data show that c-fos is increased in *BRMS1v2*$^{A273V/A273V}$ isogenic cells at a posttranslational level, which may contribute to upregulation of the putative AP-1 target genes (Fig. 3B).

Three of the putative AP-1 targets (*RAMP1, F5*, and *CEACAM6*; Fig. 3B) were validated by RT-PCR in H358 isogenic cells, H1299 V5-BRMS1v2 A273V cells, and H358 isogenic cells with or without treatment of T5224, a selective c-fos inhibitor (24) (Fig. S4E). However, only CEACAM6 protein was higher in *BRMS1v2*$^{A273V/A273V}$ isogenic cells or LUAD cells with V5-BRMS1v2 A273V, compared with H358 WT and *BRMS1v2*$^{WT/A273V}$ isogenic cells (Figs. 3, D and E, and fig. S5A) or LUAD cells with V5-BRMS1v2 WT (Fig. S5B), respectively. Whereas higher amounts of intratumoral c-fos and CEACAM6 were observed in all tested LUAD human specimens, compared with adjacent noncancerous tissues, both c-fos staining and CEACAM6 staining were more robust in *BRMS1v2*$^{A273V/A273V}$ LUAD than in *BRMS1v2*$^{WT/WT}$ or *BRMS1v2*$^{WT/A273V}$ LUAD (Fig. 3F, and fig. S5, C and D). Neither c-fos nor CEACAM6 was higher in *BRMS1v2*$^{A273V/A273V}$ noncancerous tissue or tumor stroma (Fig. S5, D and E). Additionally, the abundance of c-fos and CEACAM6 in human lung fibroblasts were not altered after co-culturing with either parental or isogenic *BRMS1v2*$^{A273V/A273V}$ cells (Fig. S5, F and G), suggesting that *BRMS1v2*$^{A273V/A273V}$ in tumor cells does not affect stromal c-fos abundance through a cell-extrinsic mechanism. Collectively, our data indicate that, although *BRMS1v2*$^{A273V/A273V}$ is a germline mutation, c-fos is increased in *BRMS1v2*$^{A273V/A273V}$ LUAD cells only, which correlates with higher amounts of *CEACAM6*.

The A273V mutant abrogates the capability of BRMS1v2 to bind and activate nuclear Src, resulting in intranuclear c-fos accumulation.

It is well established that the stability and activity of c-fos is regulated by phosphorylation(25, 26). To understand the mechanisms of increased c-fos in *BRMS1v2*$^{A273V/A273V}$ LUAD, we assessed (1) the interaction of BRMS1v2 and c-fos and (2) the phosphorylation status of c-fos. We observed that both V5-BRMS1v2 WT and A273V interact with c-fos (Fig. 4A). Whereas total and active cfos were higher and tyrosine phosphorylation of c-fos was lower in V5-BRMS1v2 A273V cells, compared with V5-BRMS1v2 WT cells (Fig. 4A). As previously described, Src directly phosphorylates tyrosines of c-fos to promote nuclear export and transcriptional repression(26). Src is in an autoinhibited state but can be activated by binding cognate ligands to its SH2 or SH3 domain(27). Analysis of BRMS1v2 using a graph kernel based tool to predict SH3-peptide interactions (https://modpepint.informatik.uni-freiburg.de/SH3PepInt/) (28) indicated that A273 is in a putative SH3-binding domain (271-285 aa) (Fig. 4B). Subsequent glutathione-S-transferase (GST) pull-downs and co-immunoprecipitations (co-IPs) showed that BRMS1v2 WT, but not A273V, interacts with Src (Fig. 4C and fig. S6A) and no other tested SH3 members (Fig. S6B). Moreover, active nuclear Src (p-Y416) was higher in H358 WT cells and LUAD cells with V5-BRMS1v2 WT, compared with H358 isogenic cells (Fig. 4D and Fig. S6C) and LUAD cells with V5-BRMS1v2 A273V, respectively (Fig. S6D). To examine whether BRMS1v2 WT binding activates Src, in vitro Src kinase assays were conducted with Src Y530M serving as control because of its lack of autoinhibition. Only GST-BRMS1v2 WT, and not GST-BRMS1v1 or GST-BRMS1v2 A273V, activated Src (Fig. 4E). Our data indicate that BRMS1v2 WT interacts with Src, resulting in Src activation, whereas BRMS1v2 A273V cannot activate Src, owing to its inability to bind Src. Use of a Src inhibitor, AZD0530, rescued c-fos expression in H358 WT cells (Supplementary Fig. 6E), proving that Src inactivation is dependent on c-fos accumulation. Additionally, higher c-fos was observed in the cytoplasm of H358 WT cells treated with a proteasome inhibitor, MG132, compared with isogenic cells (Fig. 4F), suggesting that BRMS1v2 WT-induced activation of Src promotes tyrosine phosphorylation of c-fos, resulting in c-fos nuclear exportation and degradation. In contrast, c-fos accumulates in the nuclei of *BRMS1v2*$^{A273V/A273V}$ cells because BRMS1v2 A273V cannot bind and activate Src.

CEACAM6 is a functional target of c-fos in *BRMS1v2*$^{A273V/A273V}$ LUAD.

CEACAM6 is a cell adhesion receptor of the immunoglobulin-like superfamily, and its upregulation is related to tumor progression and recurrence in multiple cancers by inducing EMT(29, 30). To confirm that *CEACAM6* transcription in *BRMS1v2*$^{A273V/A273V}$ LUAD is c-fos dependent, we used tetracycline (TCN)–inducible shRNAs targeting *FOS*. As shown in Fig. 5A, CEACAM6 was lower in *FOS* knockdown cells, confirming that c-fos regulates CEACAM6. Knockdown of Src rescued c-fos in H358 WT cells (Fig. 5B), indicating that Src inactivation results in c-fos accumulation. Unexpectedly, CEACAM6 was not rescued after Src knockdown, despite higher c-fos in H358 WT cells (Fig. 5B). Similarly, ectopic c-fos in H358 WT cells failed to induce *CEACAM6* (Fig. S7A), suggesting that c-fos regulation of *CEACAM6* is specific to *BRMS1v2*$^{A273V/A273V}$ LUAD cells.

To examine whether c-fos directly regulates *CEACAM6* in a *BRMS1v2*$^{A273V/A273V}$-dependent manner, we conducted chromatin immunoprecipitations (ChIPs) across the proximal and distal promoters of *CEACAM6* containing the putative AP-1/c-fos binding sites (Fig. S7B). Higher amounts of c-fos and c-Jun were observed on the proximal promoter of *CEACAM6* in both isogenic cells, compared with WT cells (Fig. 5C and fig. S7B). Consistent with previous findings that c-fos/c-Jun heterodimer binds more efficiently to the AP-1 site than c-Jun homodimer(23), TCN-induced *FOS* knockdown was associated with lower promoter occupancies of c-fos and c-Jun (Fig. 5C). BRMS1 was also decreased on the proximal promoter of *CEACAM6* in isogenic cells after *FOS* knockdown (Fig. 5C). To discern whether BRMS1v1 or BRMS1v2 binds to the *CEACAM6* promoter, we repeated ChIPs using V5-epitope–tagged BRMS1v2 LUAD stable cells (Fig. S2A). As expected, the V5-epitope was found only on the *CEACAM6* promoter in cells stably expressing V5-BRMS1v2 A273V (Fig. 5D). This further confirms that c-fos–induced *CEACAM6* is *BRMS1v2*$^{A273V/A273V}$ context dependent.

We next asked whether increased *CEACAM6* was associated with poor outcomes in LUAD. Examination of the TCGA LUAD cohort indicated that high *CEACAM6* is associated with poor PFS (Fig. S7C). Additionally, knockdown of *CEACAM6* in both clones of H358 isogenic *BRMS1v2*$^{A273V/A273V}$ cells significantly reduced invasion in vitro, compared with WT cells (Fig. 5E). Moreover, to evaluate the role of CEACAM6 in metastases of *BRMS1v2*$^{A273V/A273V}$ LUAD, we employed an intracardiac injection metastasis model (31), where *CEACAM6* was knocked down in H358 WT and isogenic *BRMS1v2*$^{>A273V/A273V}$ C1 cells and tumor growth was observed for 1 month post-injection. Whereas H358 isogenic *BRMS1v2*$^{A273V/A273V}$ cells exhibited higher metastatic capabilities, compared with WT cells, knockdown of *CEACAM6* reduced metastases of H358 isogenic cells (Fig. 5F). Collectively, our data demonstrate that *CEACAM6* is a functional target of c-fos in *BRMS1v2*$^{A273V/A273V}$ LUAD and that loss of *CEACAM6* ameliorates c-fos–mediated cellular invasion and metastases.

c-fos mediates invasion and metastasis of *BRMS1v2*$^{A273V/A273V}$ LUAD.

c-fos functions as a proto-oncogene by promoting tumor progression through transcriptional regulation(32). High *FOS* is associated with poor PFS among patients in the TCGA LUAD cohort (Fig. S8A). Using our TCN-inducible *FOS* shRNAs cell model (described in Fig. 5), we observed that *FOS* knockdown resulted in repression of invasion in *BRMS1v2*$^{A273V/A273V}$ isogenic cells, but not in WT cells in vitro (Fig. 6A). To evaluate the role of c-fos in metastases of *BRMS1v2*$^{A273V/A273V}$ LUAD, we re-employed the intracardiac injection metastasis model, where FOS was knocked down in H358 WT and isogenic C1 cells and tumor growth was observed for 1 month post-injection, Doxycycline diet was administrated for 1 month beginning on the injection day. As expected, in the control group, more metastases were observed in mice injected with *BRMS1v2*$^{A273V/A273V}$ isogenic cells than in mice given WT cells. In mice injected with *BRMS1v2*$^{A273V/A273V}$ cells, the metastatic burden was lower after *FOS* knockdown with doxycycline induction, compared with control (Fig. 6B). Collectively, our data indicate that increased c-fos contributes to a higher metastatic burden only in mice with *BRMS1v2*$^{A273V/A273V}$ LUAD.

c-fos is a potential therapeutic target to suppress metastases in *BRMS1v2*$^{A273V/A273V}$ LUAD.

Given the importance of c-fos in metastases of *BRMS1v2*^{A273Y,A273Y} LUAD, we sought to evaluate the efficacy of a pharmacologic strategy to inhibit c-fos using T5224, a potent c-fos inhibitor investigated in clinical trials for the treatment of intervertebral disc degeneration and rheumatoid arthritis(24, 33). Treatment with T5224 decreased invasion in isogenic cells but did not affect WT cells in vitro (Fig. S8B). To assess the efficacy of T5224 on suppression of metastasis of *BRMS1v2*$^{A273V/A273V}$ LUAD in vivo, we introduced H358 WT and isogenic C1 cells into NOG mice by intracardiac injection. T5224 or vehicle was administrated to mice for 1 month beginning on the injection day. Consistent with the previous finding (Fig. 6B), more metastases were observed in the vehicle treatment group of mice injected with H358 isogenic cells than in mice injected with WT cells at post-injection 1 month (Fig. 6C). Treatment with T5224 reduced metastases in mice with isogenic cells but did not reduce the final tumor burden in mice injected with WT cells (Fig. 6C), suggesting that T5224 effectively suppresses metastases of *BRMS1v2*$^{A273V/A273V}$ LUAD.

BRMS1v2$^{A273V/A273V}$ LUAD PDO metastatic model.

The development of PDOs represents an important advance in the modeling of human cancer(34, 35). To evaluate the anti-metastatic efficacy of T5224 in human *BRMS1v2*$^{A273V/A273V}$ LUAD, we generated PDOs from surgically resected LUAD specimens with confirmed *BRMS1v2*$^{A273V/A273V}$ (PDO-1 and PDO-2) mutations and wild type *BRMS1v2*$^{WT/WT}$ (PDO −3 and PDO −4, Fig. S8C). Whereas PDOs with *BRMS1v2*$^{A273V/A273V}$ and *BRMS1v2*$^{WT/WT}$ exhibited distinct invasion capabilities, treatment with T5224 decreased invasion of both PDOs with *BRMS1v2*$^{A273V/A273V}$ but did not significantly affect invasion of *BRMS1v2*$^{WT/WT}$ PDOs (Fig. 6D). In addition, treatment with T5224 inhibited activation of c-fos (p-c-fos S32) in all tested PDOs, but decreased CEACAM6 was only observed in *BRMS1v2*$^{A273V/A273V}$ PDOs (Fig. S8D). Collectively, these data confirm that c-fos-induced *CEACAM6* is *BRMS1v2*$^{A273V/A273V}$ context dependent and inhibition of c-fos by T5224 specifically repress invasion of *BRMS1v2*$^{A273V/A273V}$ LUAD.

To evaluate the effect of *BRMS1v2*$^{A273V/A273V}$ on metastasis in human LUAD, we used PDO-1 (*BRMS1v2*$^{A273V/A273V}$) and PDO-3 (*BRMS1v2*$^{WT/WT}$) in an in vivo intracardiac injection metastasis model. Both PDOs were generated from female patients with clinical stage IA LUAD carrying *p53* mutations (Fig. S8C). T5224 was administrated to mice injected with *BRMS1v2*$^{A273V/A273V}$ PDO-1 for 5 months beginning on the injection day. We observed that metastases occurred in mice without treatment about 4 months post-injection in both PDO groups. At the five-month completion of the experiment, 50% (4/8) and 25% (2/8) of mice injected with *BRMS1v2*$^{A273V/A273V}$ PDO-1 and *BRMS1v2*$^{WT/WT}$ PDO-3 developed metastases in different organs, respectively; however, no metastases were found in mice injected with PDO-1 (*BRMS1v2*$^{A273V/A273V}$) treated with T5224 (Fig. 6E). Assessment of total body and selected organ weights from mice injected with PDO-1 (Fig. 6F) revealed that mice without treatment had decreased total body weights and increased weights of their livers and lungs secondary to the development of metastases, compared with mice in the T5224 treatment group. Histologic analyses (Fig. 6G) at necropsy confirmed

metastases in both liver and lung of mice injected with PDO −1. These preclinical data show that targeted inhibition of c-fos using T5224, or other c-fos inhibitors, may hold promise as a therapeutic approach to clinically suppress metastases in patients with *BRMS1v2*$^{A273V/A273V}$ LUAD.

DISCUSSION

Tumor recurrence after complete resection of early-stage NSCLC occurs frequently and is associated with a poor overall survival of 30% at 5 years(36). We recently showed that higher tumor chromosomal instability, specific genomic alterations, and selected histologic subtypes contribute to the development of metastases in patients with completely resected LUAD(3). Herein, we have identified a previously undescribed germline alteration in *BRMS1*, homozygous SNP rs1052566, that is associated with the development of metastases in LUAD. We have also demonstrated that its prometastatic mechanism of action is through an increase of intratumoral c-fos that results in upregulation of *CEACAM6* (Fig. S9).

Mutation of a single copy of a proto-oncogene such as *KRAS*, is sufficient to promote tumor growth(37). In contrast, mutations in tumor suppressor genes are usually recessive, and biallelic mutations are required to convert a “normal” cell to a cancerous cell. To determine if rs 1052566 was associated with an increased risk of lung cancer we examined multiple disease-related genetic variation databases, including GWSA, ClinVar and OMIM, and found no relationship. The rs1052566 heterozygote has been shown to be associated with lymph node metastases in breast cancer(38). We found that its homozygous form (*BRMS1v2*$^{A273V/A273V}$) is associated with worse PFS in early-stage LUAD and in advanced-stage breast cancer. Similar to other tumor suppressor genes, such as *p53*(39) and *BRCAs*(40), biallelic *BRSM1v2*$^{A273V/A273V}$ results in an aggressive cancer cell phenotype as well as loss of BRMS1v2-mediated suppression of metastases.

The prevalence of homozygotes (*BRMS1v2*$^{A273V/A273V}$) is similar between the TCGA lung and breast cancer cohorts (Tables S1 and S2). Examination of the homozygote population frequency using the gnomAD database shows *BRMS1v2*$^{A273V/A273V}$ is present in 8% of individuals of European ancestry and 28% of South Asians but rarely in Africans or African Americans (Table S3). Thus, this SNP occurs at frequencies like those of well-known oncogenic drivers that are currently therapeutically targeted in LUAD.

BRMS1v2$^{A273V/A273V}$ not only abrogates the metastasis suppression function of BRMS1v2 but has a “gain of function” by mediating the gene-specific transcription of c-fos. We have shown that c-fos is higher in isogenic *BRMS1v2*$^{A273V/A273V}$ cells and LUAD. Although the results of RNA-seq indicated that most upregulated genes (73.5%) in isogenic cells were putative AP-1 targets, they make up only a small fraction of c-fos putative targets (13,087 genes; ENCODE). Moreover, *CEACAM6* was identified as a functional target of c-fos in *BRMS1v2*$^{A273V/A273V}$ cells. Most known c-fos functional targets(41), such as *DNMT1, VEGFD, MTS1*, and *EZR*, were not upregulated in *BRMS1v2*$^{A273V/A273V}$ cells. Additionally, increasing c-fos by ectopic expression or *Src* knockdown in WT cells failed

to upregulate *CEACAM6*, demonstrating that c-fos–induced transcription of *CEACAM6* is *BRMS1v2*$^{A273V/A273V}$ context dependent.

Whereas the PXXP motif is the core of SH3 domain binding sites, several structural studies have shown that not only an expanded surface of SH3 domain, but also longer peptides in the vicinity of PXXP motif contribute to the specificity of SH3 recognition (42, 43). Replacement of certain amino acids around the PXXP motif depletes the affinity of SH3 binding by altering both chemical and conformational features (44). Supporting these observations, we found that BRMS1v2 WT specifically binds to SH3 family member Src, whereas BRMS1v2 A273V fails to interact with Src. Whereas the functions of Src on the plasma membrane and cytoplasm are well known(45, 46), the role of nuclear Src in cancer is less well characterized. We have shown that nuclear Src can be activated by its interaction with BRMS1v2 WT, resulting in tyrosine phosphorylation, nuclear export, and degradation of c-fos. Alternatively, BRMS1v2 A273V loses its ability to bind Src, causing nuclear accumulation of c-fos. In support of our findings, active nuclear Src has been shown to promote phosphorylation and nuclear export of several transcription factors, including RUNX3(47), ERα(48), and YAP1(49). Moreover, we observed that activated c-fos increases transcription of *CEACAM6* and promotes metastases in *BRMS1v2*$^{A273V/A273V}$ LUAD. Thus, the inability of BRMS1v2 A273V to bind and activate Src is a critical event that contributes to metastases of *BRMS1v2*$^{A273V/A273V}$ LUAD. Our study suggests that the use of Src inhibitors in patients with *BRMS1v2*$^{A273V/A273V}$ LUAD would be ineffective and may in fact be detrimental.

The ability to recapitulate histologic, genetic and transcriptomic characteristics of the original tumor are some of the most attractive features of PDOs used in pre-clinical studies. In this study, we utilized our PDO system to assess the contribution of *BRMS1v2*$^{A273V/A273V}$ to invasion and metastases of human LUAD. To make our *BRMS1v2*$^{WT/WT}$ and *BRMS1v2*$^{A273V/A273V}$ PDOs in vivo metastasis assays comparable, we utilized PDOs generated from tumors resected from patients with the same sex, smoking histories, pathologic stage, histologic subtype, and similar mutational profiles.

Limitations of our study include evaluation of progression-free survival of *BRMS1v2*$^{A273V/A273V}$ LUAD in the TCGA LUAD cohort alone which likely does not represent the varied demographic, geographic, and genomic features observed in all patients with LUAD. Second, we employed CRIPSR knock-in to generate H358 *BRMS1v2*$^{A273V/A273V}$ isogenic cell lines as our model system. Given the complexity of oncogenic context and heterogeneity in LUAD (4), we acknowledge that more robust examination of other cells with different genomic backgrounds are needed to assess their impact on *BRMS1v2*$^{A273V/A273V}$ function. Finally, we realize that despite our efforts to match the clinicopathologic and genomic features of *BRMS1v2*$^{A273V/A273V}$ PDO-1 and *BRMS1v2*$^{WT/WT}$ PDO-3, differences in mutational profiles and tumor heterogeneity between PDOs may affect their metastatic potential.

Although most targeted therapies are tyrosine kinase inhibitors directed at somatic activating mutations or fusions, there is an increasing appreciation that targeting downstream pathways of germline mutations is a plausible therapeutic approach. Capivasertib, a pan-AKT

inhibitor, has recently been shown to be highly effective when administered to patients with breast cancer with germline *PTEN* loss-of-function mutations(50). Similarly, selected patients with NSCLC carrying *BRCA1/2* germline mutations may benefit from therapy with the PARP inhibitor Olaparib (51). Moreover, in a pan-cancer analysis, our group recently showed that 8% of patients with advanced cancer harbored a germline variant with therapeutic actionability, with 40% of these patients receiving germline genotype–directed therapy(52). Using shRNA knockdown of c-fos, or the c-fos inhibitor T5224, we successfully abrogated invasion and metastases of *BRMS1v2*$^{A273V/A273V}$ LUAD. Importantly, T5224 completely prevented metastases in *BRMS1v2*$^{A273V/A273V}$ PDOs. Additionally, we showed that knockdown of *CEACAM6*, a functional target of c-fos in *BRMS1v2*$^{A273V/A273V}$ LUAD, also decreased tumor invasion and metastases, suggesting CEACAM6 could be an alternative therapeutic target in *BRMS1v2*$^{A273V/A273V}$ LUAD (53). In fact, a phase I clinical trial investigating an anti-CEACAM6 antibody as a therapeutic in patients with solid tumors was recently completed (NCT03596372). In the recent ADAURA trial, targeting tumor-specific genomic alterations, such as activating EGFR mutations, in the adjuvant setting after surgery was shown to be highly effective at reducing tumor recurrence(54). Our findings provide robust preclinical evidence that targeting c-fos or CEACAM6 may be a feasible adjuvant therapeutic strategy to prevent and reduce metastases in patients with LUAD harboring SNP *BRMS1v2*$^{A273V/A273V}$.

MATERIALS AND METHODS

Study design

The objectives of this study were to clarify the mechanisms through which *BRMS1v2*$^{A273V/A273V}$ promotes LUAD metastases and to identify potential therapeutic targets to suppress metastases in *BRMS1v2*$^{A273V/A273V}$ LUAD. First, using the publicly available SNP datasets and TCGA cohorts of LUAD and breast cancer, we identified the prevalence and clinical relevance of *BRMS1v2*$^{A273V/A273V}$. Second, employing two distinct genetic engineered LUAD cells-based experimental systems, including LUAD cells stably expressing ectopic BRMS1v2 WT, or A273V, and LUAD homozygous *BRMS1v2*$^{A273V/A273V}$ isogenic cells by a CRISPR knock-in approach, we were able to confirm that *BRMS1v2*$^{A273V/A273V}$ enhances invasion and metastasis of LUAD cells in vitro and in vivo. Next, we performed RNA-seq., as well as a series of loss and gain of function experiments using genetic engineering and pharmacological inhibitors and found that *BRMS1v2*$^{A273V/A273V}$ promotes metastasis secondary to intratumoral accumulation of c-fos, which in turn upregulates *CEACAM6*. Finally, utilizing doxycycline-inducible shRNAs or through a c-fos specific inhibitor, T5224 used in clinical trials a) *BRMS1v2*$^{A273V/A273V}$ isogenic cells and b) PDOs with *BRMS1v2*$^{A273V/A273V}$, we confirmed that *BRMS1v2*$^{A273V/A273V}$ promotes metastases through a c-fos-dependent pro-metastatic process. Moreover, targeting c-fos reduced metastases in *BRMS1v2*$^{A273V/A273V}$ LUAD. All molecular, cellular and biochemical assays were performed with at least duplicate samples, and each experiment was repeated a minimum of two times. The metastatic capabilities of LUAD cells and PDOs were evaluated in mice. Sample sizes of each experiment were used empirically to ensure adequate statistical power and meet field standards. All animals were randomly allocated to the control and treatment groups. Tumor

measurement and treatment were not blinded, but performed by different laboratory staff. Sample sizes were determined based on statistical power analyses and ranged from 7-14 mice per group. No samples were excluded from the study. All mouse studies were carried out under the protocols approved by the Institutional Animal Care and Use Committee. Details for experimental endpoints such as in vivo experiments, number of cells used, duration of treatments, and statistical tests, are described below.

Human LUAD specimens, cell culture, antibodies, and reagents

Fresh resected human LUAD and matched adjacent noncancerous tissue were obtained after informed consent and approval by the institutional review board (16-1514, 16-107, and 12-245) at Memorial Sloan Kettering Cancer Center. Human LUAD cell lines, human lung fibroblast cells and a normal bronchial epithelial cell line (NL20) were obtained from American Type Culture Collection; Lenti-X 293T cells were purchased from Takara Bio. All cells were tested for mycoplasma. The primary antibodies used were BRMS1 (Abcam, ab134968), c-fos (Cell Signaling, #2250), c-Jun (Cell Signaling, #9165), V5-epitope (Abcam, ab15828), CEACAM6 (Santa Cruz, SC-59899), Src (Cell Signaling, #2109), p-Src Y416 (Cell Signaling, #59548), p-fos S32 (Cell Signaling, #5248), actin (Santa Cruz, sc-8432), p-Jun S63 (Cell Signaling, #2361), RAMP1 (Thermo Fisher, 10327-1-AP), and F5 (Thermo Fisher, PA5-103046). The reagents used—c-fos inhibitor T5224 (S8966) and Src inhibitor Saracatinib (AZD0530, S1006)—were purchased from Selleck Chemicals. Collagen Type IV (C6745), Collagen Type I solution (C3867), and TCN (T7760) were purchased from Millipore Sigma; puromycin (A1113803) and blasticidin (A1113903) were purchased from Thermo Fisher; CellTiter-Glo was obtained from Promega (G9241); and poly-HEMA solution was purchased from Sigma-Aldrich (P3932).

LUAD PDO culture

Fresh tissues were transported from the operating room to the laboratory and processed immediately. The tissue was minced and incubated at 37°C in 5 mL of collagenase B (5 mg/mL; Roche, #11088815001) and DNase I (100 μg/mL; Millipore Sigma, #6918230) with gentle shaking for 30 min to 1 h. The suspension was then filtered through a 70-μm nylon cell strainer (Fisher Scientific) and spun at 350 g for 5 min. The pellet was embedded in Matrigel solution (Corning, #354234) and seeded into a 48-multiwell plate (Corning, #351178). After the Matrigel had solidified, 250 μL of culture medium (Table S4) was added into each well. The PDOs were cultured in a humidity incubator at 37°C and 5% CO_2, and culture medium was changed twice per week.

Generation of *BRMS1v2*$^{A273V/A273V}$ and *BRMS1v2*$^{WT/A273V}$ isogenic cells

H358 *BRMS1v2*$^{A273V/A273V}$ isogenic cells were generated using CRISPR knock-in. Briefly, H358 cells were grown at 60%-80% confluence in a 100-mm culture dish 1 day before electroporation. On the day of electroporation, the ribonucleoprotein complexes were assembled by mixing Alt-R Cas9 nuclease (200 pmol) and Alt-R sgRNA (200 pmol; Integrated DNA Technologies). Approximately 1×10^6 cells were electroporated on the Neon transfection system using the Neon transfection system 100 μL kit (Thermo Fisher). A single-stranded oligonucleotide donor containing 172 base pairs as the homology-directed repair template was synthesized by Integrated DNA Technologies and added into the

electroporation at a concentration of 2 μM. At 2 days after electroporation, cells were diluted, and single-cell clones were generated. The sequences of sgRNA and homology-directed repair template are listed in Supplementary Table 5. The presence of SNP rs1052566 was screened by TaqMan SNP genotyping assays and confirmed by Sanger sequencing.

Total RNA isolation, RT-PCR, and RNA-seq.

Total RNA was isolated using the RNeasy mini kit (74104, Qiagen), in accordance with the manufacturer's protocol. cDNA synthesis and quantitative RT-PCRs were performed. Semiquantitative RT-PCRs were conducted using the Taq DNA polymerase kit (Qiagen, #201209). The PCR products were resolved in 1% agarose gel, and the DNA was visualized using ethidium bromide (Thermo Fisher, #10132863) under an ultraviolet transilluminator. The bands of BRMS1v2 in agarose gel were cut and dissolved using the QIAquick gel extraction kit (Qiagen, 28706X4). The sequences were confirmed by Sanger sequencing. The primers used in this study are listed in table S6.

For RNA-seq, library preparation and RNA sequencing were performed by the Integrated Genomics Operation at MSK using Illumina HiSeq with 50 paired-end reads, and approximately 30 million reads were generated for each sample. CutAdapt version cutadapt-1.6 was used to trim and filter reads. Adapters were trimmed with minimum overlap of 10 bases and reads of less than half original read length were filtered out. Trimmed sequence reads were mapped to GRC37/hg19 using the STAR (version STAR-STAR_2.5.0a) aligner 2-pass method. Expression count matrix was computed using HTSeq (version HTSeq-0.5.3). Genes with low expression in all samples (total counts <10) were filtered out, and the count matrixes were normalized using the "DESeq2" R package with default settings (adjusted $P<0.01$ and $\log_2$ FC >1).

In vivo LUAD metastasis models

Six-week-old nude mice (Jackson Laboratory, strain #002019) and NSG mice (Jackson Laboratory, strain #005557) were used in this study. All animal experiments were approved by the Animal Care and Use Committee at MSK (protocol #13-10-017). For the tail-vein injection metastasis model, 1×10^5 A549 cells stably expressing V5-BRMS1v2 WT, A273V, or control vector (n=10 mice/group) were injected into the tail veins of nude mice. For the intracardiac injection metastasis model, 1×10^5 H358 cells (*BRMS1v2*$^{WT/WT}$ and *BRMS1v2*$^{A273V/A273V}$) or isolated PDO cells were injected into the left ventricles of NSG mice. Either a doxycycline diet (0.625 g/kg; Harlan Teklad) or T5224 (150 mg/kg, oral daily) was administrated to the mice on the day of injection. Imaging was performed using an In Vivo Imaging System (IVIS) Spectrum System (PerkinElmer) 1 week after injection and repeated weekly for mice injected with LUAD cells. For mice injected with PDOs IVIS was performed 15 days after injection and repeated monthly. Metastatic burden was quantified using the value of total bioluminescence in each mouse by use of Living Image Software (version 4.2; Caliper) (55). For experiments with cell lines, an equal number of male and female mice were included in each experimental group. Mice injected with PDOs had the same sex as the patient source of the original tumor. Mice were euthanized when they approached the humane endpoint (metastatic tumor > 0.5 cm^3). The mice injected

with LUAD cells and PDOs were euthanized at 8 weeks and 5 months after injection, respectively, and necropsy was performed.

Statistical analysis

The results of all experiments represent the mean ± S.E.M. of at least 2 separate experiments. Statistical analysis was performed using Prism 9. Unpaired *t* test with Welch's correction, Fisher's exact test and the Chi-square test were used as appropriate. Progression-free survival was assessed using the Kaplan-Meier method and compared between groups using the log-rank test. A two-sided $P<0.05$ was considered to indicate statistical significance for all calculations.

Supplementary Material

Refer to Web version on PubMed Central for supplementary material.

Acknowledgments:

We thank the Integrated Genomics Operation and Antitumor Core Facility at Memorial Sloan Kettering Cancer Center for their assistance.

Funding:

This work was supported by grants from National Institutes of Health (R01CA217169 to DRJ, R01CA240472 to DRJ, R01CA236615 to PSA, R01CA192399 to MWM, T32CA009501 to JGC, and P30CA008748 to Memorial Sloan Kettering Cancer Center), Hamilton Family Foundation to DRJ, Al-Asmakh Foundation to DRJ, US Department of Defense (LC160212 to PSA), and Fiona and Stanley Druckenmiller Center for Lung Cancer Research at Memorial Sloan Kettering Cancer Center to YL.

Competing interests:

B.T.L. has served as an uncompensated advisor and consultant to Amgen, AstraZeneca, Boehringer Ingelheim, Daiichi Sankyo, Genentech, and Lilly. He has received research grants to his institution from Amgen, AstraZeneca, Bolt Biotherapeutics, Daiichi Sankyo, Genentech, Hengrui USA, and Lilly. He has received academic travel support from Jiangsu Hengrui Medicine and MORE Health but has no financial conflicts with the current work. K.O. is a cofounder of AnaNeo Therapeutics but has no financial conflict with the current work. D.R.J. serves as a consultant to AstraZeneca and is on a clinical trial steering committee for Merck – neither are related to this work. The other authors declare no competing interests.

References

1. Sung H, Ferlay J, Siegel RL, Laversanne M, Soerjomataram I, Jemal A, Bray F, Global cancer statistics 2020: GLOBOCAN estimates of incidence and mortality worldwide for 36 cancers in 185 countries. CA Cancer J Clin, (2021).
2. Rusch VW, Hawes D, Decker PA, Martin SE, Abati A, Landreneau RJ, Patterson GA, Inculet RI, Jones DR, Malthaner RA, Cohen RG, Ballman K, Putnam JB Jr., Cote RJ, Occult metastases in lymph nodes predict survival in resectable non-small-cell lung cancer: report of the ACOSOG Z0040 trial. J Clin Oncol 29, 4313–4319 (2011). [PubMed: 21990404]
3. Jones GD, Brandt WS, Shen R, Sanchez-Vega F, Tan KS, Martin A, Zhou J, Berger M, Solit DB, Schultz N, Rizvi H, Liu Y, Adamski A, Chaft JE, Riely GJ, Rocco G, Bott MJ, Molena D, Ladanyi M, Travis WD, Rekhtman N, Park BJ, Adusumilli PS, Lyden D, Imielinski M, Mayo MW, Li BT, Jones DR, A Genomic-Pathologic Annotated Risk Model to Predict Recurrence in Early-Stage Lung Adenocarcinoma. JAMA Surg 156, e205601 (2021). [PubMed: 33355651]
4. Cancer N Genome Atlas Research, Comprehensive molecular profiling of lung adenocarcinoma. Nature 511, 543–550 (2014). [PubMed: 25079552]

5. Pao W, Girard N, New driver mutations in non-small-cell lung cancer. Lancet Oncol 12, 175–180 (2011). [PubMed: 21277552]
6. Farago AF, Taylor MS, Doebele RC, Zhu VW, Kummar S, Spira AI, Boyle TA, Haura EB, Arcila ME, Benayed R, Aisner DL, Horick NK, Lennerz JK, Le LP, Iafrate AJ, Ou SI, Shaw AT, Mino-Kenudson M, Drilon A, Clinicopathologic Features of Non-Small-Cell Lung Cancer Harboring an NTRK Gene Fusion. JCO Precis Oncol 2018, (2018).
7. de Alencar VTL, Formiga MN, de Lima VCC, Inherited lung cancer: a review. Ecancermedicalscience 14, 1008 (2020). [PubMed: 32104210]
8. Parry EM, Gable DL, Stanley SE, Khalil SE, Antonescu V, Florea L, Armanios M, Germline Mutations in DNA Repair Genes in Lung Adenocarcinoma. J Thorac Oncol 12, 1673–1678 (2017). [PubMed: 28843361]
9. Hu Z, Huo X, Lu D, Qian J, Zhou J, Chen Y, Xu L, Ma H, Zhu J, Wei Q, Shen H, Functional polymorphisms of matrix metalloproteinase-9 are associated with risk of occurrence and metastasis of lung cancer. Clin Cancer Res 11, 5433–5439 (2005). [PubMed: 16061858]
10. Xie C, Yang L, Yang X, Yang R, Li Y, Qiu F, Chen M, Fang W, Bin X, Deng J, Huang D, Liu B, Zhou Y, Lu J, Sipa1 promoter polymorphism predicts risk and metastasis of lung cancer in Chinese. Mol Carcinog 52 Suppl 1, E110–117 (2013). [PubMed: 23661532]
11. Avan A, Maftouh M, Avan A, Tibaldi C, Zucali PA, Giovannetti E, SNPs in PI3K-PTEN-mTOR and brain metastases in NSCLC--letter. Clin Cancer Res 20, 3623–3624 (2014). [PubMed: 24803580]
12. Li Q, Wu H, Chen B, Hu G, Huang L, Qin K, Chen Y, Yuan X, Liao Z, SNPs in the TGF-beta signaling pathway are associated with increased risk of brain metastasis in patients with non-small-cell lung cancer. PLoS One 7, e51713 (2012). [PubMed: 23284751]
13. Li X, Xu X, Fang J, Wang L, Mu Y, Zhang P, Yao Z, Ma Z, Liu Z, Rs2853677 modulates Snail1 binding to the TERT enhancer and affects lung adenocarcinoma susceptibility. Oncotarget 7, 37825–37838 (2016). [PubMed: 27191258]
14. Smith PW, Liu Y, Siefert SA, Moskaluk CA, Petroni GR, Jones DR, Breast cancer metastasis suppressor 1 (BRMS1) suppresses metastasis and correlates with improved patient survival in non-small cell lung cancer. Cancer Lett 276, 196–203 (2009). [PubMed: 19111386]
15. Slipicevic A, Holm R, Emilsen E, Ree Rosnes AK, Welch DR, Maelandsmo GM, Florenes VA, Cytoplasmic BRMS1 expression in malignant melanoma is associated with increased disease-free survival. BMC Cancer 12, 73 (2012). [PubMed: 22356677]
16. Phadke PA, Vaidya KS, Nash KT, Hurst DR, Welch DR, BRMS1 suppresses breast cancer experimental metastasis to multiple organs by inhibiting several steps of the metastatic process. Am J Pathol 172, 809–817 (2008). [PubMed: 18276787]
17. Liu Y, Smith PW, Jones DR, Breast cancer metastasis suppressor 1 functions as a corepressor by enhancing histone deacetylase 1-mediated deacetylation of RelA/p65 and promoting apoptosis. Mol Cell Biol 26, 8683–8696 (2006). [PubMed: 17000776]
18. Meehan WJ, Samant RS, Hopper JE, Carrozza MJ, Shevde LA, Workman JL, Eckert KA, Verderame MF, Welch DR, Breast cancer metastasis suppressor 1 (BRMS1) forms complexes with retinoblastoma-binding protein 1 (RBP1) and the mSin3 histone deacetylase complex and represses transcription. J Biol Chem 279, 1562–1569 (2004). [PubMed: 14581478]
19. Liu Y, Mayo MW, Nagji AS, Hall EH, Shock LS, Xiao A, Stelow EB, Jones DR, BRMS1 suppresses lung cancer metastases through an E3 ligase function on histone acetyltransferase p300. Cancer Res 73, 1308–1317 (2013). [PubMed: 23269275]
20. Alexandrova EM, Mirza SA, Xu S, Schulz-Heddergott R, Marchenko ND, Moll UM, p53 loss-of-heterozygosity is a necessary prerequisite for mutant p53 stabilization and gain-of-function in vivo. Cell Death Dis 8, e2661 (2017). [PubMed: 28277540]
21. Liberzon A, Birger C, Thorvaldsdottir H, Ghandi M, Mesirov JP, Tamayo P, The Molecular Signatures Database (MSigDB) hallmark gene set collection. Cell Syst 1, 417–425 (2015). [PubMed: 26771021]
22. Huang da W, Sherman BT, Lempicki RA, Systematic and integrative analysis of large gene lists using DAVID bioinformatics resources. Nat Protoc 4, 44–57 (2009). [PubMed: 19131956]

23. Halazonetis TD, Georgopoulos K, Greenberg ME, Leder P, c-Jun dimerizes with itself and with c-Fos, forming complexes of different DNA binding affinities. Cell 55, 917–924 (1988). [PubMed: 3142692]
24. Aikawa Y, Morimoto K, Yamamoto T, Chaki H, Hashiramoto A, Narita H, Hirono S, Shiozawa S, Treatment of arthritis with a selective inhibitor of c-Fos/activator protein-1. Nat Biotechnol 26, 817–823 (2008). [PubMed: 18587386]
25. Sasaki T, Kojima H, Kishimoto R, Ikeda A, Kunimoto H, Nakajima K, Spatiotemporal regulation of c-Fos by ERK5 and the E3 ubiquitin ligase UBR1, and its biological role. Mol Cell 24, 63–75 (2006). [PubMed: 17018293]
26. Ferrero GO, Velazquez FN, Caputto BL, The kinase c-Src and the phosphatase TC45 coordinately regulate c-Fos tyrosine phosphorylation and c-Fos phospholipid synthesis activation capacity. Oncogene 31, 3381–3391 (2012). [PubMed: 22105363]
27. Brown MT, Cooper JA, Regulation, substrates and functions of src. Biochim Biophys Acta 1287, 121–149 (1996). [PubMed: 8672527]
28. Kundu K, Mann M, Costa F, Backofen R, MoDPepInt: an interactive web server for prediction of modular domain-peptide interactions. Bioinformatics 30, 2668–2669 (2014). [PubMed: 24872426]
29. Maraqa L, Cummings M, Peter MB, Shaaban AM, Horgan K, Hanby AM, Speirs V, Carcinoembryonic antigen cell adhesion molecule 6 predicts breast cancer recurrence following adjuvant tamoxifen. Clin Cancer Res 14, 405–411 (2008). [PubMed: 18223215]
30. Chen J, Li Q, An Y, Lv N, Xue X, Wei J, Jiang K, Wu J, Gao W, Qian Z, Dai C, Xu Z, Miao Y, CEACAM6 induces epithelial-mesenchymal transition and mediates invasion and metastasis in pancreatic cancer. Int J Oncol 43, 877–885 (2013). [PubMed: 23857344]
31. Er EE, Valiente M, Ganesh K, Zou Y, Agrawal S, Hu J, Griscom B, Rosenblum M, Boire A, Brogi E, Giancotti FG, Schachner M, Malladi S, Massague J, Pericyte-like spreading by disseminated cancer cells activates YAP and MRTF for metastatic colonization. Nat Cell Biol 20, 966–978 (2018). [PubMed: 30038252]
32. Weekes D, Kashima TG, Zandueta C, Perurena N, Thomas DP, Sunters A, Vuillier C, Bozec A, El-Emir E, Miletich I, Patino-Garcia A, Lecanda F, Grigoriadis AE, Regulation of osteosarcoma cell lung metastasis by the c-Fos/AP-1 target FGFR1. Oncogene 35, 2852–2861 (2016). [PubMed: 26387545]
33. Makino H, Seki S, Yahara Y, Shiozawa S, Aikawa Y, Motomura H, Nogami M, Watanabe K, Sainoh T, Ito H, Tsumaki N, Kawaguchi Y, Yamazaki M, Kimura T, A selective inhibition of c-Fos/activator protein-1 as a potential therapeutic target for intervertebral disc degeneration and associated pain. Sci Rep 7, 16983 (2017). [PubMed: 29208967]
34. Gao D, Vela I, Sboner A, Iaquinta PJ, Karthaus WR, Gopalan A, Dowling C, Wanjala JN, Undvall EA, Arora VK, Wongvipat J, Kossai M, Ramazanoglu S, Barboza LP, Di W, Cao Z, Zhang QF, Sirota I, Ran L, MacDonald TY, Beltran H, Mosquera JM, Touijer KA, Scardino PT, Laudone VP, Curtis KR, Rathkopf DE, Morris MJ, Danila DC, Slovin SF, Solomon SB, Eastham JA, Chi P, Carver B, Rubin MA, Scher HI, Clevers H, Sawyers CL, Chen Y, Organoid cultures derived from patients with advanced prostate cancer. Cell 159, 176–187 (2014). [PubMed: 25201530]
35. Kim M, Mun H, Sung CO, Cho EJ, Jeon HJ, Chun SM, Jung DJ, Shin TH, Jeong GS, Kim DK, Choi EK, Jeong SY, Taylor AM, Jain S, Meyerson M, Jang SJ, Patient-derived lung cancer organoids as in vitro cancer models for therapeutic screening. Nat Commun 10, 3991 (2019). [PubMed: 31488816]
36. Brandt WS, Bouabdallah I, Tan KS, Park BJ, Adusumilli PS, Molena D, Bains MS, Huang J, Isbell JM, Bott MJ, Jones DR, Factors associated with distant recurrence following R0 lobectomy for pN0 lung adenocarcinoma. J Thorac Cardiovasc Surg 155, 1212–1224 e1213 (2018). [PubMed: 29246549]
37. Burgess MR, Hwang E, Mroue R, Bielski CM, Wandler AM, Huang BJ, Firestone AJ, Young A, Lacap JA, Crocker L, Asthana S, Davis EM, Xu J, Akagi K, Le Beau MM, Li Q, Haley B, Stokoe D, Sampath D, Taylor BS, Evangelista M, Shannon K, KRAS Allelic Imbalance Enhances Fitness and Modulates MAP Kinase Dependence in Cancer. Cell 168, 817–829 e815 (2017). [PubMed: 28215705]
38. Roberts MR, Hong CC, Edge SB, Yao S, Bshara W, Higgins MJ, Freudenheim JL, Ambrosone CB, Case-only analyses of the associations between polymorphisms in the metastasis-modifying genes

BRMS1 and SIPA1 and breast tumor characteristics, lymph node metastasis, and survival. Breast Cancer Res Treat 139, 873–885 (2013). [PubMed: 23771732]

39. Donehower LA, Harvey M, Slagle BL, McArthur MJ, Montgomery CA Jr., Butel JS, Bradley A, Mice deficient for p53 are developmentally normal but susceptible to spontaneous tumours. Nature 356, 215–221 (1992). [PubMed: 1552940]
40. Elledge SJ, Amon A, The BRCA1 suppressor hypothesis: an explanation for the tissue-specific tumor development in BRCA1 patients. Cancer Cell 1, 129–132 (2002). [PubMed: 12086871]
41. Eferl R, Wagner EF, AP-1: a double-edged sword in tumorigenesis. Nat Rev Cancer 3, 859–868 (2003). [PubMed: 14668816]
42. Kami K, Takeya R, Sumimoto H, Kohda D, Diverse recognition of non-PxxP peptide ligands by the SH3 domains from p67(phox), Grb2 and Pex13p. EMBO J 21, 4268–4276 (2002). [PubMed: 12169629]
43. Teyra J, Huang H, Jain S, Guan X, Dong A, Liu Y, Tempel W, Min J, Tong Y, Kim PM, Bader GD, Sidhu SS, Comprehensive Analysis of the Human SH3 Domain Family Reveals a Wide Variety of Non-canonical Specificities. Structure 25, 1598–1610 e1593 (2017). [PubMed: 28890361]
44. Gemperle J, Hexnerova R, Lepsik M, Tesina P, Dibus M, Novotny M, Brabek J, Veverka V, Rosel D, Structural characterization of CAS SH3 domain selectivity and regulation reveals new CAS interaction partners. Sci Rep 7, 8057 (2017). [PubMed: 28808245]
45. Zhang SQ, Yang W, Kontaridis MI, Bivona TG, Wen G, Araki T, Luo J, Thompson JA, Schraven BL, Philips MR, Neel BG, Shp2 regulates SRC family kinase activity and Ras/Erk activation by controlling Csk recruitment. Mol Cell 13, 341–355 (2004). [PubMed: 14967142]
46. Garcia R, Bowman TL, Niu G, Yu H, Minton S, Muro-Cacho CA, Cox CE, Falcone R, Fairclough R, Parsons S, Laudano A, Gazit A, Levitzki A, Kraker A, Jove R, Constitutive activation of Stat3 by the Src and JAK tyrosine kinases participates in growth regulation of human breast carcinoma cells. Oncogene 20, 2499–2513 (2001). [PubMed: 11420660]
47. Kang KA, Piao MJ, Ryu YS, Maeng YH, Hyun JW, Cytoplasmic Localization of RUNX3 via Histone Deacetylase-Mediated SRC Expression in Oxidative-Stressed Colon Cancer Cells. J Cell Physiol 232, 1914–1921 (2017). [PubMed: 27990641]
48. Arnold SF, Vorojeikina DP, Notides AC, Phosphorylation of tyrosine 537 on the human estrogen receptor is required for binding to an estrogen response element. J Biol Chem 270, 30205–30212 (1995). [PubMed: 8530431]
49. Ege N, Dowbaj AM, Jiang M, Howell M, Hooper S, Foster C, Jenkins RP, Sahai E, Quantitative Analysis Reveals that Actin and Src-Family Kinases Regulate Nuclear YAP1 and Its Export. Cell Syst 6, 692–708 e613 (2018). [PubMed: 29909276]
50. Kingston B, Bailleux C, Delaloge S, Schiavon G, Scott V, Lacroix-Triki M, Carr TH, Kozarewa I, Gevensleben H, Kemp Z, Pearson A, Turner N, Andre F, Exceptional Response to AKT Inhibition in Patients With Breast Cancer and Germline PTEN Mutations. JCO Precis Oncol 3, (2019).
51. Diossy M, Sztupinszki Z, Borcsok J, Krzystanek M, Tisza V, Spisak S, Rusz O, Timar J, Csabai I, Fillinger J, Moldvay J, Pedersen AG, Szuts D, Szallasi Z, A subset of lung cancer cases shows robust signs of homologous recombination deficiency associated genomic mutational signatures. NPJ Precis Oncol 5, 55 (2021). [PubMed: 34145376]
52. Stadler ZK, Maio A, Chakravarty D, Kemel Y, Sheehan M, Salo-Mullen E, Tkachuk K, Fong CJ, Nguyen B, Erakky A, Cadoo K, Liu Y, Carlo MI, Latham A, Zhang H, Kundra R, Smith S, Galle J, Aghajanian C, Abu-Rustum N, Varghese A, O'Reilly EM, Morris M, Abida W, Walsh M, Drilon A, Jayakumaran G, Zehir A, Ladanyi M, Ceyhan-Birsoy O, Solit DB, Schultz N, Berger MF, Mandelker D, Diaz LA Jr., Offit K, Robson ME, Therapeutic Implications of Germline Testing in Patients With Advanced Cancers. J Clin Oncol 39, 2698–2709 (2021). [PubMed: 34133209]
53. Hong KP, Shin MH, Yoon S, Ji GY, Moon YR, Lee OJ, Choi SY, Lee YM, Koo JH, Lee HC, Lee GK, Kim SR, Lee KH, Han HS, Choe KH, Lee KM, Hong JM, Kim SW, Yi JH, Ji HJ, Kim YB, Song HG, Therapeutic effect of anti CEACAM6 monoclonal antibody against lung adenocarcinoma by enhancing anoikis sensitivity. Biomaterials 67, 32–41 (2015). [PubMed: 26204223]
54. Jones DR, Wu YL, Tsuboi M, Herbst RS, Targeted therapies for resectable lung adenocarcinoma: ADAURA opens for thoracic oncologic surgeons. J Thorac Cardiovasc Surg, (2021).

55. Liu Y, Amin EB, Mayo MW, Chudgar NP, Bucciarelli PR, Kadota K, Adusumilli PS, Jones DR, CK2alpha' Drives Lung Cancer Metastasis by Targeting BRMS1 Nuclear Export and Degradation. Cancer Res 76, 2675–2686 (2016). [PubMed: 26980766]

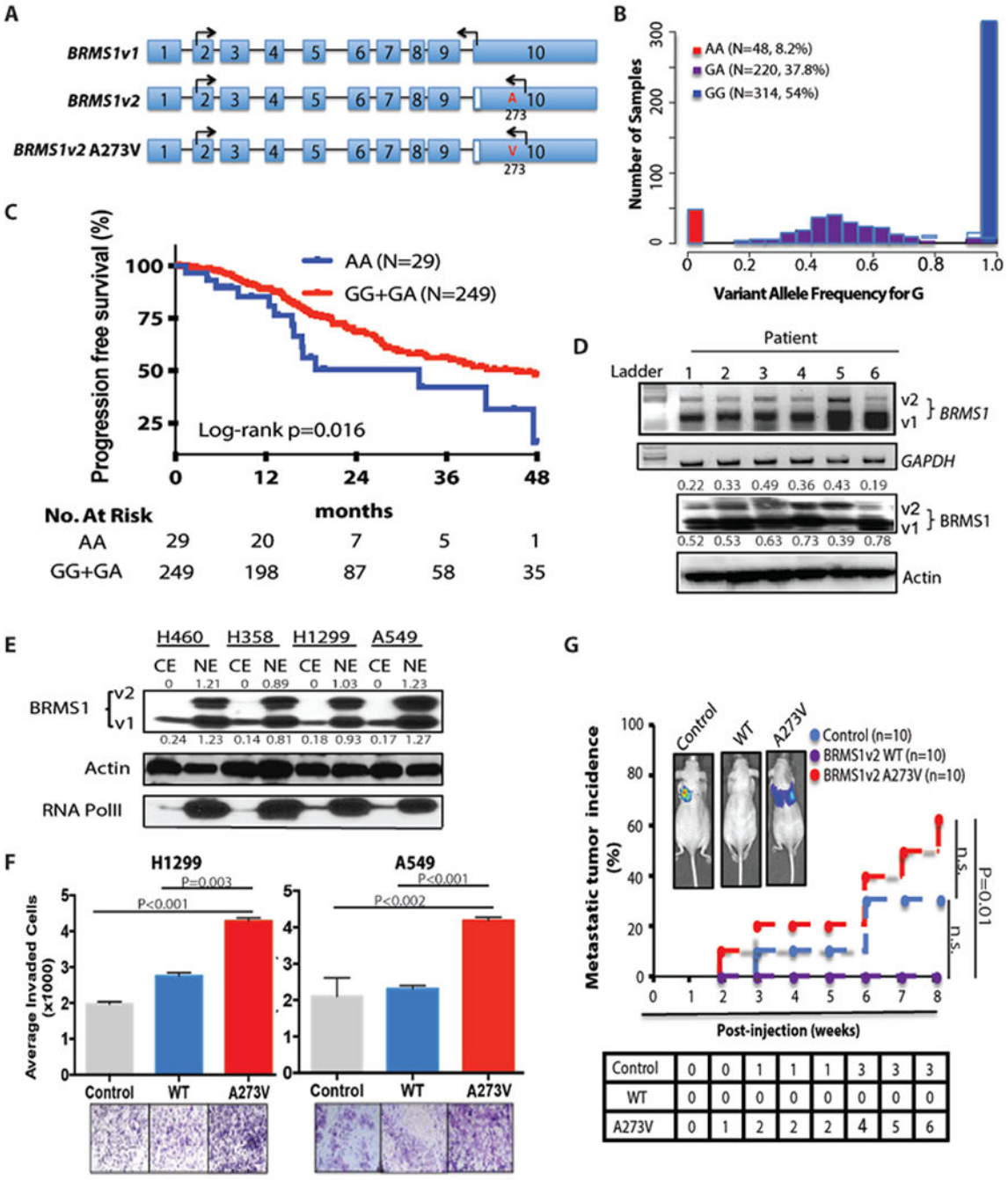

Control	0	0	1	1	1	3	3	3
WT	0	0	0	0	0	0	0	0
A273V	0	1	2	2	2	4	5	6

Fig. 1. BRMS1v2 A273V caused by SNP rs1052566 enhances risk of LUAD metastases.

A) Schematic illustration of the transcripts of *BRMS1* variants 1 and 2. Blue squares: exons; left arrows: positions of translation start codon; right arrows: positions of translation stop codon; red letters "A" and "V": the codon 273 of BRMS1v2 . **B)** Histogram of G allele frequency in the TCGA LUAD cohort (n=582). **C)** Kaplan-Meier plot of PFS for stages I-II LUAD (n=278) from the TCGA LUAD cohort. **D)** (Top) Semiquantitative RT-PCRs indicating mRNAs of *BRMS1v1* and *v2*. (Bottom) Immunoblots showing proteins of BRMS1v1 and v2 in 6 human LUAD specimens. Densitometry of each band were

normalized to the corresponding Actin (numbers on the top line for BRMS1v2; numbers on the bottom line for BRMS1v1). **E)** BRMS1v1 and v2 were detected by immunoblot using isolated cytosolic extract (CE) and nuclear extract (NE) of the indicated LUAD cell lines. **F)** Invasion chamber assays using LUAD cell lines stably expressing V5-BRMS1v2 WT or A273V. **G)** The indicated A549 stable cells were injected into the tail vein of nude mice. (Top) Cumulative incidence curves of metastatic tumor for the indicated cell lines measured by In Vivo Imaging System. *P* values were calculated using Fisher's exact test. n.s. = not significant. (Bottom) Table indicating the number of mice with lung metastases.

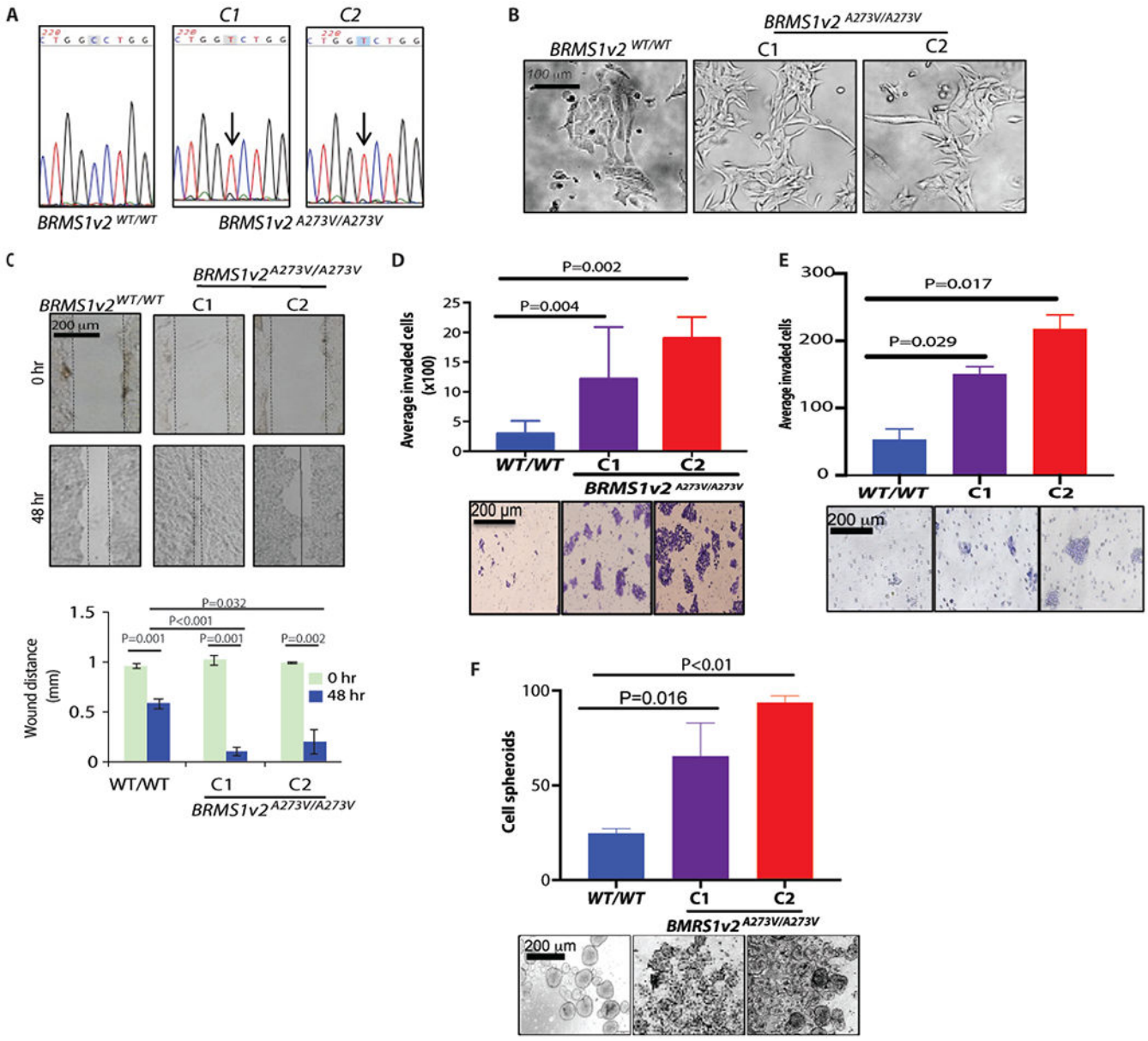

Fig. 2. Homozygous *BRMS1v2*$^{A273V/A273V}$ promotes migration and invasion of LUAD cells in vitro.

A) Sequencing chromatograms showing genomic DNA around BRMS1v2 A273 in H358 parental (*BRMS1v2*$^{WT/WT}$) cells and two clones of isogenic *BRMS1v2*$^{A273V/A273V}$ cells, C1 and C2. Arrows indicating the peaks of C>T. **B)** Phase-contrast images showing cell morphologic appearance of H358 parental (*BRMS1v2*$^{WT/WT}$) cells and two clones of isogenic *BRMS1v2*$^{A273V/A273V}$ cells, C1 and C2. **C)** (Top) Photographs showing the representative scratch wounds using H358 cells. (Bottom) Bar graph indicating the average distances of scratch wounds at 0 and 48 h. **D)** (Top) Bar graph and (Bottom) representative images showing the average numbers of invaded cells of H358 cell lines in 2-D culturing in invasion chamber assays. **E)** (Top) Bar graph and (Bottom) representative images showing the invasion capabilities of H358 cells 1 week after culture in a 3-D hanging drop system. **F)**

(Top) Bar graph and (Bottom) representative images showing the formation of cell spheroids of H358 parental (*BRMS1v2*$^{WT/WT}$) and isogenic cells (C1 and C2).

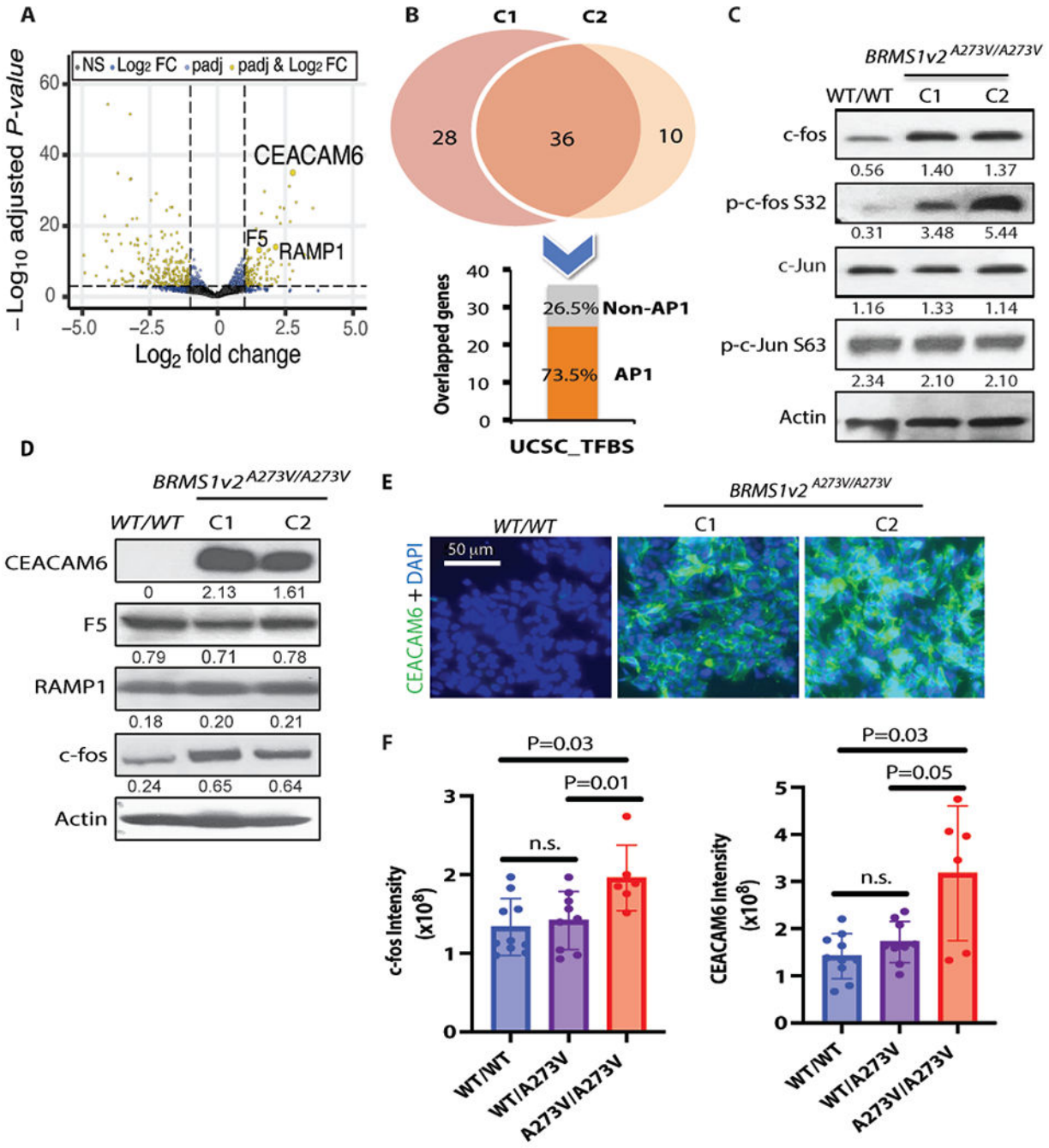

Fig. 3. c-fos is higher in isogenic *BRMS1v2*$^{A273V/A273V}$ cells.

A) Volcano plot showing the genes differentially expressed in isogenic cell clones, C1 and C2, and WT cells RNA-seq.. Red dots: $\log_2$ FC >1 and adjusted P<0.05; blue dots: $\log_2$ FC <1 but adjusted P<0.05; green dots: $\log_2$ FC >1 but adjusted P>0.05; gray dots: $\log_2$ FC <1 and adjusted P>0.05. **B)** Venn diagram (Top) showing genes upregulated in isogenic *BRMS1v2*$^{A273V/A273V}$ cells. The bar graph (Bottom) represents the results of transcription factors binding signature (UCSC TFBS) analyses for the upregulated genes overlapping between C1 and C2 cells. **C)** Western blots showing total and active c-fos and c-Jun proteins

in H358 parental cells and isogenic *BRMS1v2*$^{A273V/A273V}$ cells. Densitometry of each band normalized to the corresponding Actin was labeled under the blots. **D)** Immunoblots showing the expression of the indicated proteins in H358 cell lines. Densitometry of each band normalized to the corresponding Actin was labeled under the blots. **E)** Immunofluorescences indicating the cellular expression of CEACAM6 (green) in H358 cell lines. Blue: DAPI nuclear staining. **F)** Bar graphs showing staining intensity of intratumoral c-fos (Left) and CEACAM6 (Right) in immunohistochemistry for human specimens with *BRMS1v2*$^{WT/WT}$ (n=10), *BRMS1v2*$^{WT/A273V}$ (n=9), and *BRMS1v2*$^{A273V/A273V}$ (n=6), n.s. = not significant.

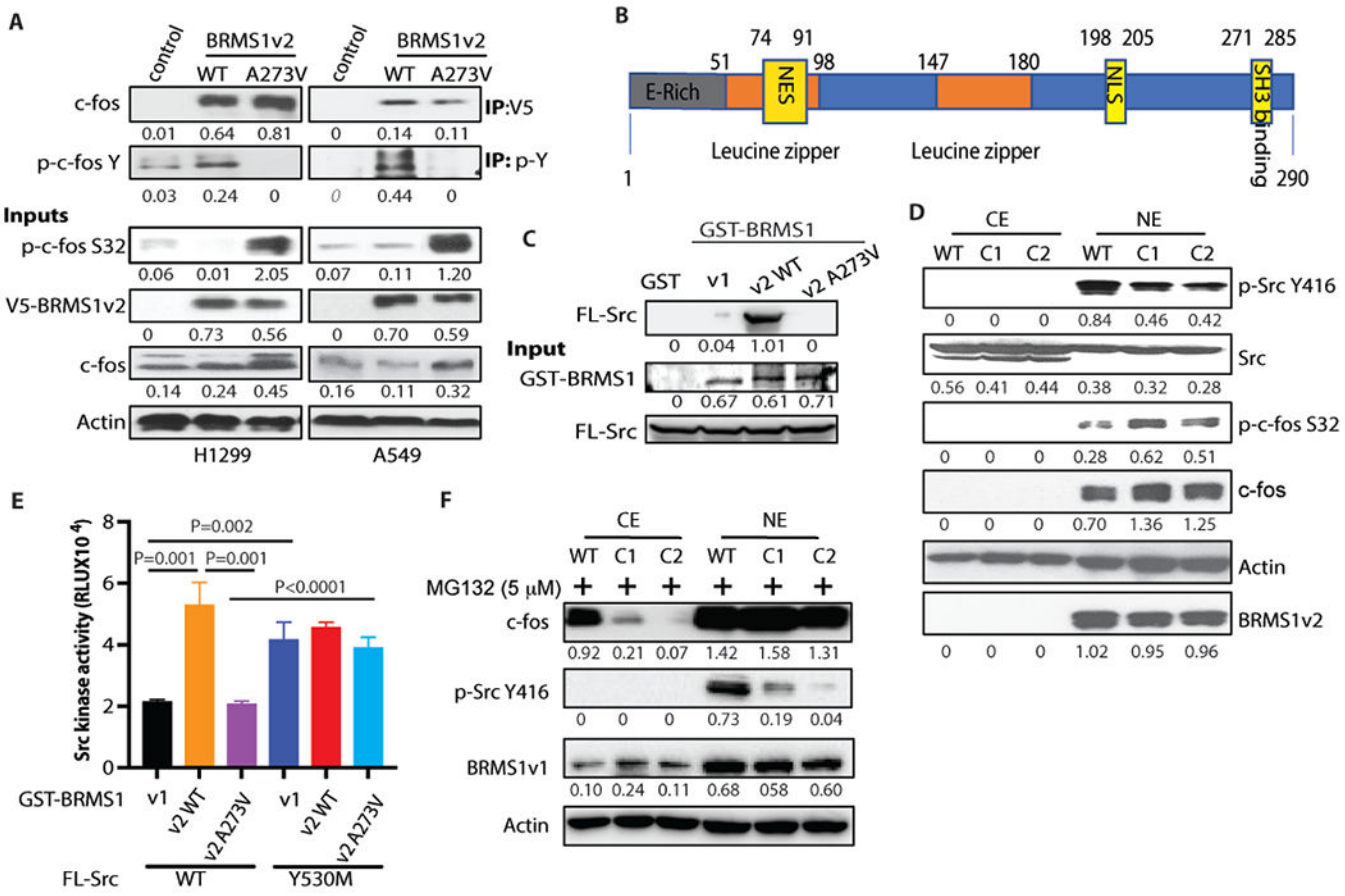

Fig. 4. Inactive nuclear Src results in c-fos accumulation in isogenic *BRMS1v2*$^{A273V/A273V}$ cells.

A) Co-IPs using V5-epitope tag or phospho-pan-tyrosine (p-Y) antibody in LUAD cells stably expressing V5- BRMS1v2 WT or A273V and c-fos in immunoprecipitation complexes. The indicated proteins were detected as inputs. Densitometry of each band normalized to the corresponding Actin was labeled under the blots. **B)** Schematic illustration of the domains in BRMS1v2. Green box: the glutamic-rich region (E-rich); orange boxes: predicted imperfect leucine zippers motifs; purple box: predicted nuclear export signal (NES); yellow box: predicted nuclear localization signal (NLS); red box: predicted SH3 binding domain. **C)** FLAG-Src (FL-Src) was pulled down by the indicated Glutathione S Transferase (GST)-fusion proteins, and the presence of FL-Src in the complexes was detected by immunoblot. Densitometry of each band normalized to the corresponding FL-Src was labeled under the blots. **D)** Immunoblots detecting the indicated proteins in nuclear extract (NE) and cytosolic extract (CE) of H358 cell lines. Densitometry of each band normalized to the corresponding Actin was labeled under the blots. **E)** Bar graph indicating the kinase activities of FL-Src WT and Y530M in the presence of the indicated GST-fusion proteins. **F)** Immunoblots showing c-fos in the cytoplasm extract (CE) and nuclear extract (NE) of H358 cell lines treated with MG132 (5 μM) for 16 h. Densitometry of each band normalized to the corresponding Actin was labeled under the blots. RLU, relative light unit.

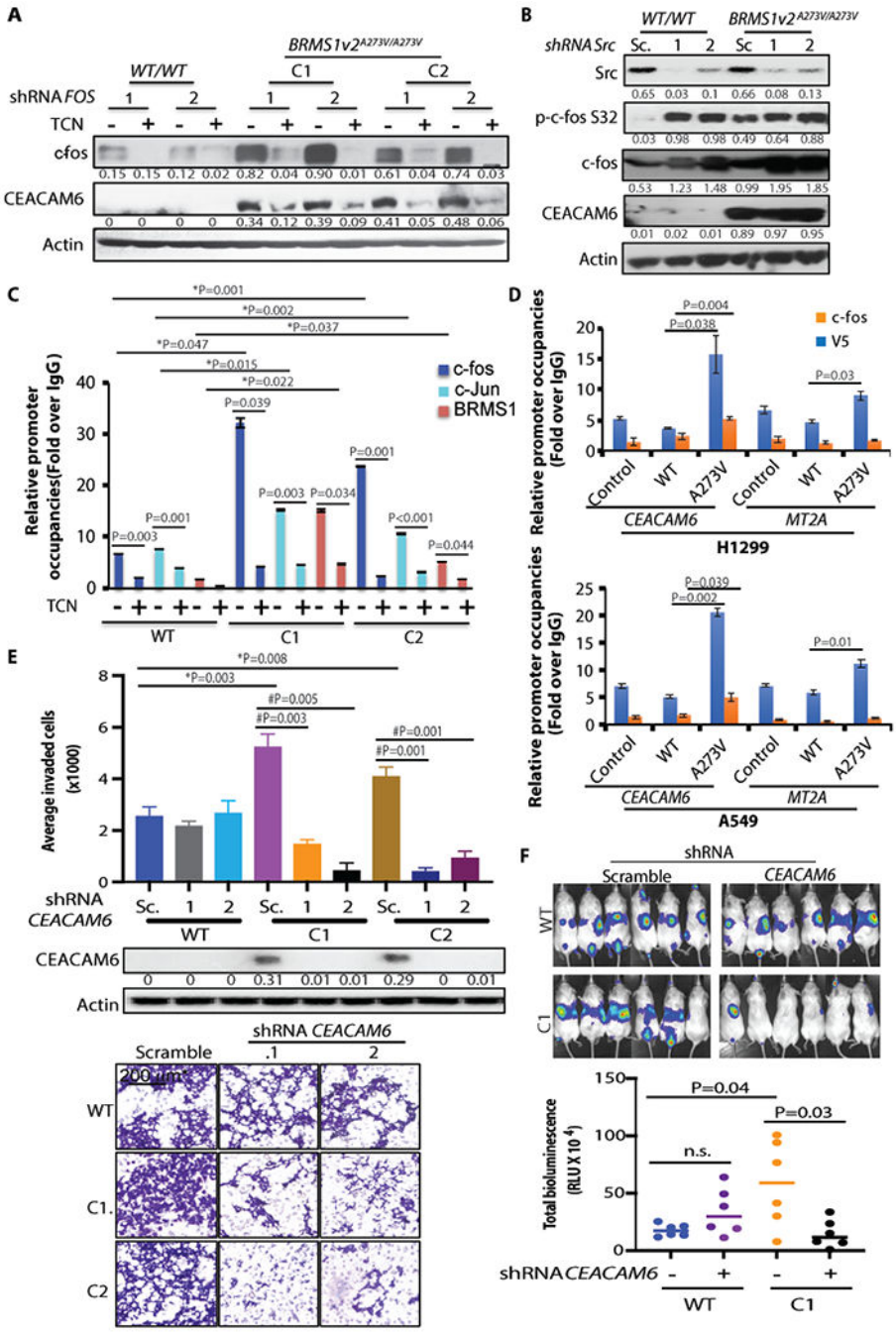

Fig. 5. *CEACAM6* is a target that mediates c-fos–induced invasion in *BRMS1v2*$^{A273V/A273V}$ LUAD.

A) Immunoblots displaying the expression of c-fos and CEACAM6 after H358 cell lines with Tet-on–controlled shRNAs *FOS* were treated with or without TCN (10 μg/mL) for 48 h. Densitometry of each band normalized to the corresponding Actin was labeled under the blots. **B)** Immunoblots displaying the expression of the indicated proteins in H358 parental (WT) cells and isogenic C1 cells with shRNAs *Src* or scramble sequence (Sc). Densitometry of each band normalized to the corresponding Actin was labeled under the blots. **C)** H358

cells with Tet-on–controlled shRNA *FOS1* were treated with or without TCN (10 μg/mL) for 48 h. ChIPs were performed across the proximal promoter of *CEACAM6* using antibodies against c-fos, c-Jun, or BRMS1. * comparisons between C1 or C2 and WT cells/without TCN. **D)** ChIPs were performed using LUAD cells stably expressing V5-BRMS1v2 WT or A273V across the proximal promoter of *CEACAM6* and *MT2A* promoters using antibodies against c-fos, c-Jun, or V5-epitope. **E)** Bar graph (Top) and representative images (Bottom) showing average numbers of invaded cells of H358 cells with shRNAs *CEACAM6* or scramble sequence (Sc) in invasion chamber assays. * comparisons between C1/Sc or C2/Sc and WT cells/Sc. # comparisons between the same cells with different shRNA and Sc. Immunoblots (Middle) displaying the knockdown efficiency of individual shRNA. **F)** H358 cells with shRNA *CEACAM6* were introduced into NSG mice (n=6/group) by intracardiac injection. Bioluminescent images (Top) showing metastases in mice and scatter plot (Bottom) indicating the total bioluminescence (region of interest [ROI]) of each mouse at post-injection 1 month.

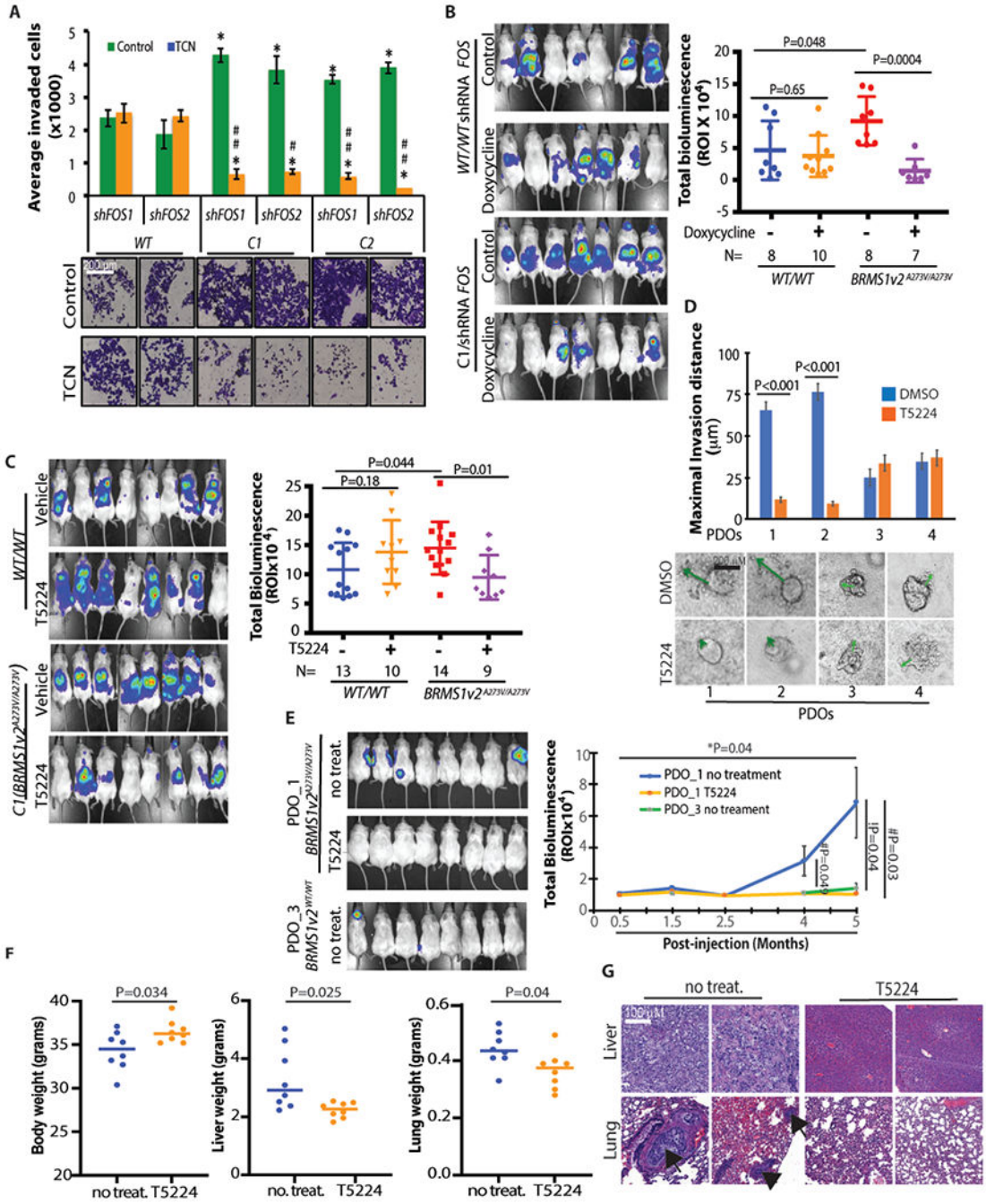

Fig. 6. Genetically or pharmacologically targeting c-fos reduces metastasis in *BRMS1v2*$^{A273V/A273V}$ LUAD in mice.

A) Bar graph showing average invaded cells of H358 cells with shRNAs *FOS* with or without TCN (10 μg/mL) for 48 h. **P*<0.05 compared with the same shRNA *FOS*–infected WT cells without TCN (control). #*P*<0.05 and ##*P*<0.01 compared with the same cell line without TCN. **B)** H358 cells with shRNA *FOS1* were introduced into NSG mice by intracardiac injection. Doxycycline or regular diet was administrated. Bioluminescent images (Left) showing metastases in representative mice at post-injection

1 month and scatter plot (Right) indicating the total bioluminescence (region of interest [ROI]) of each mouse. **C)** H358 cells were introduced into NSG mice by intracardiac injection, and T5224 or vehicle (control, 20% polyvinylpyrrolidone) was administrated daily 1 month after inoculation. Bioluminescent images (Left) showing metastases in representative mice at post-injection 1 month and scatter plot (Right) displaying the total bioluminescence (ROI) of each mouse. **D)** PDO-1 and −2 (*BRMS1v2*$^{A273V/A273V}$) and PDO-3 and −4 (*BRMS1v2*$^{WT/WT}$) were treated with T5224 or DMSO, and 3-D invasion assays performed. The maximal invasion distance (μm) was determined from n=20 PDOs/group. Arrows: the farthest invaded cell.**E), F)** and **G)** PDO-1 (*BRMS1v2*$^{A273V/A273V}$) or PDO-3 (*BRMS1v2*$^{WT/WT}$) was introduced into NSG female mice by intracardiac injection (n=8/group), and T5224 was administrated to mice injected with PDO-1 daily 5 months after inoculation. **E)** Bioluminescent images (Top) showing metastases in the experimental mice over time and line graph (Bottom) indicating the average total bioluminescence (region of interest [ROI], mean ± S.E.M.) of each mouse at the indicated months post-injection. * comparison between PDO-1 no treatment at post-injection 0.5 month and 5 months, # comparisons between PDO-1 with T5224 treatment and no treatment at post-injection 4 and 5 months, ! comparison between PDO-1 no treatment and PDO-3 no treatment at post-injection 5 months. **F)** Scatter plots showing the total body weight (left), liver weight (middle) and lung weight (right) of each mouse in both treatment groups at 5 months. **G)** Hematoxylin and eosin staining of lungs and livers from mice at necropsy. Arrows indicate micrometastases in the lungs.